

## A Comparison between Sinusoidal Oscillation and Constant Temperature Boundary Conditions in Annulus Filled with Porous Media Saturated with Nanofluid

Dr. Manal H. AL – Hafidh

Mechanical Engineering Department, University of Baghdad/ Baghdad

Email: Manalhadi2005@yahoo.com

### ABSTRACT

A numerical study has been carried out to investigate the heat transfer by natural convection of nanofluid taking copper as nano particles and the water as based fluid in a three dimensional annulus enclosure filled with porous media between two horizontal concentric cylinders with 12 annular fins of 3mm length and 2.4 mm thickness attached to the inner cylinder under steady state condition and different wall temperature boundary conditions. The governing equations which used are continuity, momentum and energy equations under an assumptions used Darcy law and Boussinesq's approximation which are transformed to dimensionless equations. The finite difference approach is used to obtain all the computational results using the MATLAB- 7. The parameters affected on the system are modified Rayleigh number ( $10 \leq Ra^* \leq 500$ ), radius ratio  $R_r$  (0.293, 0.365 and 0.435) and the volume fraction ( $0 \leq \phi \leq 0.3$ ). The results show that, increasing of fin length decreases the heat transfer rate and for  $Ra^* < 100$ , decreasing  $R_r$  cause to decrease  $Nu$  and adding Cu nanoparticles with  $\phi = 0.35$  cause 27.9% enhancement in heat transfer. A correlation for  $Nu$  in terms of  $Ra$ ,  $H_f$  and  $\phi$ , has been developed for inner hot cylinder.

**Keywords:** Three Dimensional Annulus, Laminar Flow, Natural Convection, Nanofluid, Porous Media.

### مقارنة بين درجة الحرارة الثابتة والمتغيرة جيبيًا لظروف تخوم محتوى حلقي مملوء بوسط مسامي مشبع بمائع النانو

#### الخلاصة:

أجريت في هذا البحث دراسة عددية لإنتقال الطاقة الحرارية بالحمل الحر لمائع نانو باستخدام جسيمات نانو النحاس Cu في الماء كمائع أساس في فجوة حلقيّة ثلاثية الأبعاد مملوءة بوسط مسامي بين أسطوانتين أفقيتين متحدتي المركز بوجود 12 زعنفة بطول 3mm وسمك 2.4 mm متصلة بالإسطوانة الداخلية تحت شروط حالة الإستقرار. المعادلات الحاكمة هي معادلة الاستمرارية والزخم والطاقة. كُتبت المعادلات تحت فرضيات قانون دارسي وتقريب بوسنسك وتحويلها إلى معادلة بدلالة الجهد المتجه والتي بدورها حُلّت عدديًا باستخدام طريقة الفروق المحددة ثم

استخدام برنامج MATLAB-7 لإيجاد النتائج الحسابية. العناصر الإستدلالية المؤثرة هي عدد رايلى المعدل (10  $\leq Ra^* \leq 500$ ) وزمن لابعدي ثابت  $\tau'=0.2$  والسعة الابعدية ( $0 \leq a \leq 0.8$ ) وكسر الحجوم ( $0 \leq \phi \leq 0.3$ ). بينت النتائج تعزيز في معدل انتقال الطاقة الحرارية للظروف الحدبة لدرجة الحرارة المتغيرة جيبيًا وتعزيز إضافي عند إضافة جسيمات النانو. تزداد نسبة عدد نسلت (NUR) بزيادة  $Ra^*$  حتى تصل قيمة ثابتة عند  $Ra^* > 100$ . مثلت النتائج بمعادلة تجريبية للأسطوانة الداخلية الساخنة تربط عدد نسلت بعدد رالي المعدل كسر الحجوم والسعة الابعدية.

## INTRODUCTION

Coupled heat and mass transfer driven by buoyancy due to temperature and concentration variations in fluid-saturated porous media has been of growing interest during the last several decades because of its great practical applications in modern industry, such as the design of building components for energy consideration, control of pollutant spread in groundwater, compact heat exchangers, solar power collectors and food industries [1]. For the first time **Lage and Bejan, 1993** [2] investigated the buoyancy driven flows in a square enclosure with periodic heat flux and examined the effects of oscillation frequency of heat generation on natural convection. Other researchers carried out similar studies by considering a clear base fluid within the enclosure as in [3] and [4]. **Choi, 1995**[5] showed that introducing nanofluids containing nanoparticles with substantially higher thermal conductivities improves the heat transfer performance. The results of this study have also been confirmed by other researchers [6–8]. **Mina et al., 2011**[9] Studied numerically laminar conjugate heat transfer by natural convection and conduction in a vertical annulus formed between an inner heat generating solid circular cylinder and an outer isothermal cylindrical boundary. It is assumed that the two sealed ends of the tube to be adiabatic. The governing equations have been solved using the finite volume approach, using SIMPLE algorithm on the collocated arrangement.

**Ghasemi and Aminossadati, 2010** [10] Examined the periodic natural convection in an enclosure filled with nanofluids. Whilst a heat source with oscillating heat flux is located on the left wall of the enclosure, the right wall is maintained at a relatively low temperature and the other walls are thermally insulated. The utilization of nanoparticles, in particular Cu, enhances the heat transfer especially at low Rayleigh numbers. In addition, the oscillation period of heat generation affects the maximum operational temperature of the heat source.

**Mostafa and Seyed, 2012** [11] investigated numerically Natural convection fluid flow and heat transfer inside C-shaped enclosures filled with Cu-Water nanofluid using finite volume method and SIMPLER algorithm. It was found from the obtained results that the mean Nusselt number increased with increase in Rayleigh number and volume fraction of Cu nanoparticles regardless aspect ratio of the enclosure. Moreover the obtained results showed that the rate of heat transfer increased with decreasing the aspect ratio of the cavity. Also it was found that the rate of heat transfer increased with increase in nanoparticles volume fraction.

**Kuang and Angela, 2010**[12] Analyzed the heat transfer and fluid flow of natural convection in a cavity filled with  $Al_2O_3$ / water nanofluid that operates under differentially heated walls. The heat transfer rates are examined for parameters of

non-uniform nanoparticle size, mean nanoparticle diameter, nanoparticle volume fraction, Prandtl number, and Grashof number.

Heat transfer and fluid flow due to buoyancy forces in a partially heated enclosure using nanofluids is carried out by **Hakan, Oztop and Abu-Nada, 2008 [13]** using different types of nanoparticles. The flush mounted heater is located to the left vertical wall with a finite length. The temperature of the right vertical wall is lower than that of heater while other walls are insulated. The finite volume technique is used to solve the governing equations.

**Mohammadreza et al., 2011[14]** Investigated the heat transfer performance in an enclosure including nanofluids with a localized heat source. The hydrodynamics and thermal fields are coupled together using the Boussinesq's approximation.

In the present study, the heat transfer by natural convection of nanofluid taking copper as nano particles and the water as based fluid in a three dimensional annulus enclosure filled with porous media between two horizontal concentric cylinders under steady state condition and for thermal boundary condition of two cases constant or sinusoidal temperature oscillation at the wall of the inner cylinder and for modified Rayleigh number ( $10 \leq Ra^* \leq 500$ ), radius ratio  $R_r$  (0.293, 0.365 and 0.435) and the volume fraction ( $0 \leq \phi \leq 0.3$ ).

**Mathematical Model**

The effective thermal conductivity of the nano-fluid is approximated by Maxwell-Garnetts model:

$$\frac{k_{nf}}{k_f} = \frac{k_s + 2k_f - 2\phi (k_f - k_s)}{k_s + 2k_f + \phi (k_f - k_s)} \dots(1)$$

The use of this equation is restricted to spherical nano-particles where it does not account for other shapes of nano-particles. This model is found to be appropriate for studying heat transfer enhancement using nanofluid [9, 15].

The thermo-physical properties of pure water and nanoparticles are given in **Table (1) [10]**.

**Table (1) Thermo-physical properties of pure fluid and nanoparticles**

physical properties	Pure water	Cu
P(kg/m <sup>3</sup> )	997.1	8933
Cp(J/kg K)	4179	385
K(W/m K)	0.613	400
B(1/K)	21x10 <sup>-5</sup>	1.67x10 <sup>-5</sup>

The viscosity of the nanofluid can be approximated as viscosity of a base fluid  $\mu_f$  containing dilute suspension of fine spherical particles and is given by [16]:

$$\mu_{nf} = \frac{\mu_f}{(1-\phi)^{2.5}} \quad \dots(2)$$

The governing equations used are continuity, momentum and energy equations which are transformed to dimensionless equations and the vector potential equation was obtained in the dimensionless form as [17] and [18]:

$$\frac{\partial U_r}{\partial R} + \frac{U_r}{R} + \frac{1}{R} \frac{\partial U_\phi}{\partial \phi} + \frac{\partial U_z}{\partial Z} = 0 \quad \dots (3)$$

$$Ra^* Pr * C_1 * \left( \sin \phi \frac{\partial \theta}{\partial Z} \right) = \frac{\frac{\partial^2 \psi_r}{\partial R^2} - \frac{1}{R^2} \frac{\partial (R \psi_r)}{\partial R} - \frac{2}{R} \frac{\partial \psi_r}{\partial R} - \frac{1}{R^2} \frac{\partial^2 \psi_r}{\partial \phi^2}}{\frac{\partial^2 \psi_r}{\partial Z^2} - \frac{2}{R} \frac{\partial \psi_z}{\partial Z}} \quad \dots (4)$$

$$Ra^* Pr C_1 * \left( \cos \phi \frac{\partial \theta}{\partial Z} \right) = \frac{-\frac{\partial^2 \psi_\phi}{\partial Z^2} - \frac{\partial^2 \psi_\phi}{\partial R^2} - \frac{1}{R^2} \frac{\partial^2 \psi_\phi}{\partial \phi^2}}{-\frac{2}{R^2} \frac{\partial \psi_r}{\partial \phi} + \frac{\psi_\phi}{R^2} - \frac{1}{R} \frac{\partial \psi_\phi}{\partial R}} \quad \dots (5)$$

$$-\frac{Ra^* Pr C_1}{\alpha_{nf}} \left( \frac{1}{R} \cos \phi \frac{\partial \theta}{\partial \phi} + \sin \phi \frac{\partial \theta}{\partial R} \right) = \frac{-\frac{\partial^2 \psi_z}{\partial R^2} - \frac{1}{R} \frac{\partial \psi_z}{\partial R}}{-\frac{1}{R^2} \frac{\partial^2 \psi_z}{\partial \phi^2} - \frac{\partial^2 \psi_z}{\partial Z^2}} \quad \dots(6)$$

Where

$$C_1 = \frac{\alpha_f}{\alpha_{nf}} \left[ (1-\phi) + \phi \frac{(\rho\beta)_s}{(\rho\beta)_f} \right] (1-\phi)^{2.5} \quad \dots(7)$$

And the energy equation will be:

$$\begin{aligned} & \left( \frac{1}{R} \frac{\partial \psi_z}{\partial \phi} - \frac{\partial \psi_\phi}{\partial Z} \right) \frac{\partial \theta}{\partial R} + \frac{1}{R} \left( \frac{\partial \psi_r}{\partial Z} - \frac{\partial \psi_z}{\partial R} \right) \frac{\partial \theta}{\partial \phi} \\ & + \left( \frac{\psi_\phi}{R} + \frac{\partial \psi_\phi}{\partial R} - \frac{1}{R} \frac{\partial \psi_r}{\partial \phi} \right) \frac{\partial \theta}{\partial Z} \qquad \dots(8) \\ & = \frac{\alpha_{nf}}{r_2} \left[ \frac{\partial^2 \theta}{\partial R^2} + \frac{1}{R} \frac{\partial \theta}{\partial R} + \frac{1}{R^2} \frac{\partial^2 \theta}{\partial \phi^2} + \frac{\partial^2 \theta}{\partial Z^2} \right] \end{aligned}$$

And fin equation will be [12]:

$$\frac{\partial \theta}{\partial R} + \frac{\theta}{R} + \frac{1}{R} \frac{\partial \theta}{\partial \phi} + \frac{\partial \theta}{\partial Z} = 0 \qquad \dots(9)$$

For the vector potential field, the boundary conditions are given in figure (1).

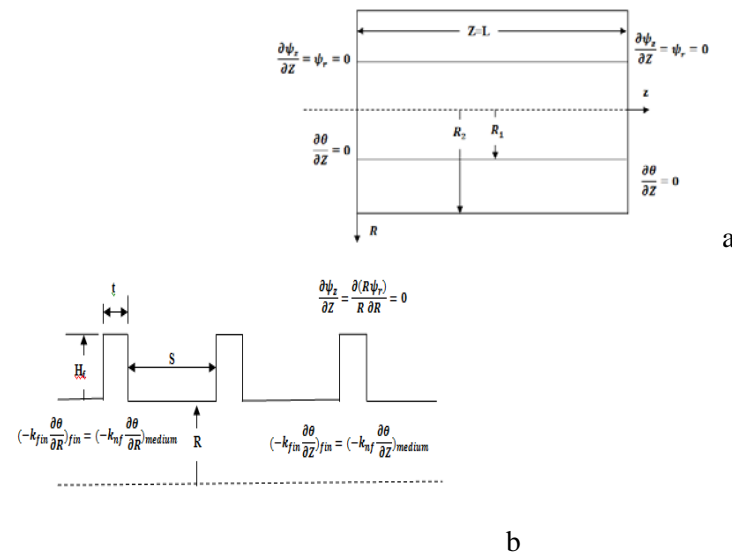


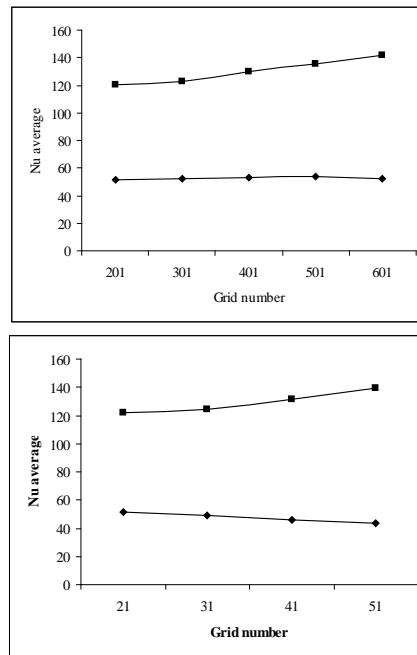
Figure (1) a. Annulus boundary conditions

b. Fins boundary conditions

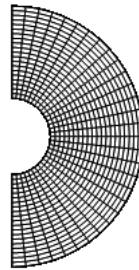
**Computational Technique**

The equations were transformed into the finite difference approximation, where the upwind differential method in the left hand side of the energy equation and the centered – space differential method for the other terms were used, and solved by using (SOR) method [10].

A computer program was built using MATLAB to meet the requirements of the problem. The value of the vector potential  $\psi$  calculated at each node, in which the value of vector potential is unknown, the other node will appear in the right hand side of each equation.



a



b

Figure (2) a. Grid Size Study for point at the inner hot cylinder, b. grid generation in the R-φ section

Figure (2) illustrates the influence of number of grid points for a test case of  $Ra^* = 500$ ,  $a=0.8$ ,  $\eta=0.01$  and  $\phi = 0.3$ . The figure shows the average Nusselt number for point located on the inner hot cylinder. The number of grid points used was 21 grid points in the R – direction, 31 in the  $\phi$  – direction and 301 in the Z – direction.

**Dimensionless Hydraulic Boundary Conditions:**

$$\frac{1}{R} \frac{\partial}{\partial R} (R\psi) = 0 \quad \text{at } R = R_1, 1$$

$$\frac{\partial \psi}{\partial Z} = 0 \quad \text{at } Z = 0, L$$

And for the fin, the boundary conditions are given as:

$$\frac{1}{R} \frac{\partial}{\partial R} (R \psi_r) = \frac{\partial \psi_z}{\partial Z} = 0$$

On the fin faces which were located on the following planes:

At  $R = R_1$  for (fin base)

At  $r = r_1 + H_f$  for (fin top)

**Dimensionless Thermal Boundary Conditions:**

$$\theta = 0 \quad \text{at } R = R_2 = 1$$

Case 1: constant wall temperature

$$\theta = 1 \quad \text{at } R = R_1 = r_{in} / r_{out}$$

Case 2:

$$\theta = 1 + a \sin(2\pi \tau' / \eta') \quad \text{at } R = R_1 = r_{in} / r_{out}$$

$$\frac{\partial \theta}{\partial Z} = 0 \quad \text{at } Z = 0, L$$

At  $R = H_1$

$$-k_{fin} \frac{\partial \theta}{\partial R} \Big|_{fin} = -k_{nf} \frac{\partial \theta}{\partial R} \Big|_{nf}$$

At  $S_1$  for any R and  $S_2$  for any R

$$-k_{fin} \frac{\partial \theta}{\partial Z} \Big|_{fin} = -k_{nf} \frac{\partial \theta}{\partial Z} \Big|_{nf}$$

**Calculation of The Local and Average Nusselt Number**

The local Nusselt number  $Nu_1$  and  $Nu_2$  on the inner and the outer cylinders are written in the form:

$$Nu_1 = -(1 - R_1) \frac{k_{nf}}{k_f} \left( \frac{\partial \theta}{\partial R} \right)_{R=R_1} \quad \dots(11)$$

$$Nu_2 = -(1 - R_1) \frac{k_{nf}}{k_f} \left( \frac{\partial \theta}{\partial R} \right)_{R=1} \quad \dots(12)$$

The average Nusselt number  $Nu_{in}$  and  $Nu_{out}$  on the inner and the outer cylinders are defined as:

$$Nu_{in} = -(1 - R_1) \frac{1}{\pi L} \int_0^L \int_0^\pi \left( \frac{\partial \theta}{\partial R} \right)_{R=R} d\phi dZ \quad \dots (13)$$

$$Nu_{out} = -(1 - R_1) \frac{1}{\pi L} \int_0^L \int_0^\pi \left( \frac{\partial \theta}{\partial R} \right)_{R=1} d\phi dZ \quad \dots (14)$$

The effect of the nanofluids on heat transfer rate introduced as a variable called Nusselt number ratio (NUR) with its definition given as:

$$NUR = \frac{Nu_{out|nanofluid}}{Nu_{out|pure fluid}} \quad \dots (15)$$

A correlation for Nu in terms of Ra,  $\phi$  and dimensionless amplitude (a) has been developed for inner hot cylinder as follow:

$$Nu = 13.07 (Ra^*)^{0.4304} \phi^{0.533} a^{0.4003}$$

## RESULTS AND DISCUSSION

### Temperature, streamlines and velocity Fields

The dimensionless temperature distribution and the axial velocity within the enclosure is presented in a contour map form. For isotherms, one section was selected in the (Z-R) plane along the length of the annulus, and the other in the (R- $\phi$ ) plane, in a manner allowed studying the temperature distribution and streamlines within each plane. For comparison purposes, parameters are selected of constant wall temperature,  $Ra^*=500$  and  $\phi=0$  in Fig.(3) and  $\phi=0.3$  in Fig. (4). Fig.(3) shows the temperature distribution for pure fluid where the isotherms shift towards the outer (cold) cylinder and a thicker cold layer in the lower region of the annulus wall exist while a high temperature exist in the upper half of the annulus where the waviness in temperature distribution is due to the existence of the fins. Fig. (4) illustrates the enhancement in heat transfer where the temperature decrease clearly in the regions between fins. For the streamlines it can be seen from figures that one vortices occur which indicates that the heated flow moves up from the inner heated cylinder of the enclosure and impinges to the cold outer cylinder. The difference between nanofluid and pure fluid cases are the higher intensity of streamlines in nanofluid. The velocity field shows a clear decrease in the axial velocity due to the enhancement in heat transfer caused the fluid to be cooled and as a result the velocity decreased.

For sinusoidal oscillation in the inner cylinder wall temperature, a selected case is taken for dimensionless amplitude  $a= 0.8$ ,  $\eta=0.01$ ,  $Ra^*=500$ ,  $\phi=0$  in Fig.(5) and  $\phi=0.3$  in Fig. (6). Fig.(5) shows the temperature distribution for pure fluid and that the increase in amplitude cause to enhance heat transfer so the values of isotherms decrease and a decrease in the axial velocity and

streamlines intensity observed. In Fig. (6) as  $\phi$  increase to 0.3 an extra enhancement in heat transfer obtained and the enclosure cooled with more decrease in the velocity and streamlines intensity.

Figures (7) and (8) illustrate the variation of Local Nusselt number along the length of the inner cylinder. It is clear from these figures, as mentioned previously that heat transfer enhances by sinusoidal oscillation boundary condition and adding nano particles to the pure fluid causes extra enhancement in heat transfer.

The variation of the average Nu with the modified Rayleigh number for various volume fractions ( $\phi$ ) and with various wall temperatures boundary condition is illustrated in Fig. (9). This figure shows that for  $Ra^*=10$ , as the volume fraction increase from zero to 0.3 the enhancement percent in heat transfer is 1.327% for constant wall temperature and 1.42% for sinusoidal oscillation boundary condition for amplitude equal 0.8.

Figure (10) shows the variation of the average Nu with the modified Rayleigh number for various dimensionless amplitudes in pure fluid and in nanofluid with volume fraction  $\phi = 0.3$ . For constant wall temperature with  $Ra^*=10$ , as the dimensionless amplitude increase from zero to 0.8 the enhancement percent in heat transfer is 0.78 % where in nanofluid with  $\phi=0.3$  the enhancement percent is 0.857 %.

The variation of the average Nusselt number with the dimensionless period  $\eta$  for dimensionless amplitude  $a=0.8$  and  $Ra^*=300$  is shown in Fig. (11); where it is clear that Nu decrease with the increase of the dimensionless period  $\eta$ .

Fig. (12) shows that the Nusselt number ratio (NUR) increase with the modified Rayleigh number increase until  $Ra^*$  equal about 100 and then the values (for various volume fractions ( $\phi$ ) and  $a=0.8$ ) reach a steady state. In Fig. (13) the variation of the Nusselt number ratio with the dimensionless amplitude ( $a$ ) for various volume fractions ( $\phi$ ) and  $Ra^*=500$  is illustrated and it is clear that NUR is nearly constant with the dimensionless amplitude and increase when adding more copper particles.

## CONCLUSION

From the present work results and for the annulus that described previously, the following conclusions can be obtained:

- 1- The increase in the dimensionless amplitude cause to enhance heat transfer which causes the values of the isotherms to decrease and as consequent a decrease in the axial velocity values and the streamlines intensity observed.
- 2- Adding copper particles to the pure fluid cause an extra enhancement in heat transfer and the enclosure cooled with more decrease in the velocity and streamlines intensity.
- 3- For  $Ra^*=10$ , as the volume fraction increase from zero to 0.3 the enhancement percent in heat transfer is 1.327% for constant wall temperature and 1.42% for sinusoidal oscillation boundary condition.

- 4- For constant wall temperature with  $Ra^*=10$ , as the dimensionless amplitude increase from zero to 0.8 the enhancement percent in heat transfer is 0.78 % where in nanofluid the enhancement percent is 0.857 %.
- 5- As  $Ra^*$  increase, the Nusselt number ratio (NUR) increase until  $Ra^*$  equal about 100 where it reaches a constant value.

## REFERENCES

- [1] Ching Y. C., Soret and Dufour effects on heat and mass transfer by natural convection from a vertical truncated cone in a fluid-saturated porous medium with variable wall temperature and concentration, *International Communications in Heat and Mass Transfer* 37 (2010) 1031–1035
- [2] Lage J.L., Bejan A., The resonance of natural convection in an enclosure heated periodically from the side, *Int. J. Heat Mass Transf.* 36 (8) (1993) 2027–2038
- [3] Kwak H.S., Kuwahara K., Jae Min H., Resonant enhancement of natural convection heat transfer in a square enclosure, *Int. J. Heat Mass Transf.* 41 (18) (1998) 2837–2846.
- [4] Kwak H.S., Hyun J.M., Natural convection in an enclosure having a vertical sidewall with time-varying temperature, *J. Fluid Mech.* 329 (1996) 65–88.
- [5] Choi S.U.S., Enhancing thermal conductivity of fluids with nanoparticles, *ASME Fluids Eng. Div.* 231 (1995) 99–105.
- [6] Khanafer K., Vafai K., Lightstone M., Buoyancy-driven heat transfer enhancement in a two-dimensional enclosure utilizing nanofluids, *Int. J. Heat Mass Transf.* 46 (19) (2003) 3639–3653.
- [7] Jou R.Y., Tzeng S.C., Numerical research of nature convective heat transfer enhancement filled with nanofluids in rectangular enclosures, *Int. Comm. Heat Mass Transf.* 33 (6) (2006) 727–736.
- [8] Nnanna A.G.A., Experimental model of temperature-driven nanofluid, *J. Heat Transf.* 129 6 (2007) 697–704.
- [9] Mina S., Amir H. M., Farhad T., A numerical investigation of conjugated-natural convection heat transfer enhancement of a nanofluid in an annular tube driven by inner heat generating solid cylinder, *Int. communication of Heat and Mass Transfer*, 38(2011) 533 – 542 .
- [10] Ghasemi B., Aminossadati S.M., Periodic natural convection in a nanofluid-filled enclosure with oscillating heat flux, *International Journal of Thermal Sciences* 49 (2010) 1–9.
- [11] Mostafa M., Seyed M. H., Numerical study of natural convection of a nanofluid in C-shaped enclosures, *International Journal of Thermal Sciences* 55 (2012) 76-89
- [12] Kuang C. L., Violi A., Natural convection heat transfer of nanofluids in a vertical cavity: Effects of non-uniform particle diameter and temperature on thermal conductivity, *International Journal of Heat and Fluid Flow* 31 (2010) 236–245
- [13] Hakan F. O., Eiyad A.N., Numerical study of natural convection in partially heated rectangular enclosures filled with nanofluids, *International Journal of Heat and Fluid Flow* 29 (2008) 1326–1336

[14] Mohammadreza N., Ebrahim S., Mohammad H. R., Investigation of heat transfer enhancement in an enclosure filled with nanofluids using multiple relaxation time lattice Boltzmann modeling, International Communications in Heat and Mass Transfer 38 (2011) 128–138

[15] Nazar R., Tham L., Pop I., Ingham D. B., Mixed Convection Boundary Layer Flow from a Horizontal Circular Cylinder Embedded in a Porous Medium Filled with a Nanofluid, Transp Porous Med (2011) 86:517–536

[16] Esmaeilpour M., Abdollahzadeh M., Free convection and entropy generation of nanofluid inside an enclosure with different patterns of vertical wavy walls, International Journal of Thermal Science 52 (2012)127-136

[17] Wang B. X. and Zhang X., Natural Convection in Liquid Saturated Porous Media Between Concentric Inclined Cylinders, Int. J. Heat and Mass Transfer Vol. 33. No 5, pp. 827-833, 1990.

[18] Fukuda K., Takata Y., Hasegawa S., Shimomura H. and Sanokawa K., Three – Dimensional Natural Convection in a Porous Medium Between Concentric Inclined Cylinders, Proc. 19<sup>th</sup> Natl Heat Transfer Conf., Vol. HTD – 8, pp. 97 – 103, 1980.

**Nomenclature**

**Latin Symbols**

Symbol	Description	Units
$a$	Dimensionless amplitude( $a=$ amplitude/ temperature difference of cylinders wall)	—
$C_p$	Specific heat at constant pressure	kJ/kg°C
$Da$	Darcy number $Da=K/r^2$	
$g$	Acceleration due to gravity	m/s <sup>2</sup>
$H_f$	Fin length	m
$H_l$	Dimensionless fin length ( $H_f/ r_{out}$ )	—
$k_{fin.}$	Fin thermal conductivity	W/m K
$k_f$	Thermal conductivity of the fluid	W/m K

$k_s$	Thermal conductivity of the solid	W/m K
$k_{nf}$	Thermal conductivity of nanofluid	W/m K
$K$	Permeability	$m^2$
$L$	Dimensionless length of the cylinder	—
$r_{in}$	Radius of the inner cylinder	m
$r_{out}$	Radius of the outer cylinder	m
$R$	Dimensionless radial coordinate	
$R_1$	Dimensionless radius for inner cylinder	m
$R_2$	Dimensionless radius for outer cylinder	m
$Ra^*$	Modified Rayleigh number $Ra^* = Ra Da$	—
$Ra$	Rayleigh number	
$s$	Fin spacing (fin pitch)	m
$S_1$	Dimensionless fin spacing $S_1 = \frac{s}{2 r_{out}}$	—
$S_2$	Dimensionless fin spacing $S_2 = \frac{\frac{s}{2} + t}{r_{out}}$	—
$U_r$	Dimensionless velocity component in R -direction	—
$U_\phi$	Dimensionless	

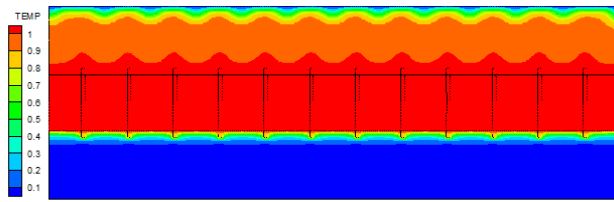
	velocity component in $\emptyset$ -direction	—
$U_z$	Dimensionless velocity component in Z - direction	—
Z	Dimensionless axial coordinate	—

**Greek Letters**

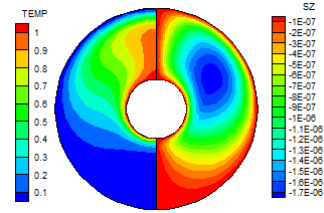
Symbol	Description	Units
$\alpha_f$	Thermal diffusivity of fluid	$m^2/s$
$\alpha_{nf}$	thermal diffusivity of nanofluid	$m^2/s$
$\beta$	Volumetric thermal expansion coefficient	1/K
$\theta$	Dimensionless temperature	—
$\mu_f$	Dynamic viscosity of fluid	$N.s/m^2$
$\mu_{nf}$	Dynamic viscosity of nanofluid	$N.s/m^2$
$\psi_r$	Streamline in radial direction	—
$\psi_\emptyset$	Streamline in angular direction	—
$\psi_z$	Streamline in axial direction	—
$\hat{t}$	Dimensionless time $\hat{t} = \text{time} \times \alpha_f / R^2$	—
$\hat{\eta}$	Dimensionless period $\hat{\eta} = \text{period} \times \alpha_f / R^2$	—

Subscripts

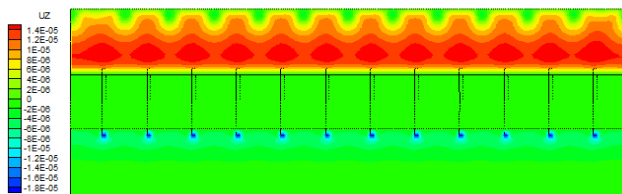
Symbol	Description	Units
$( )_f$	Fluid	--
$( )_s$	Solid	--



a. Isotherms along annulus length

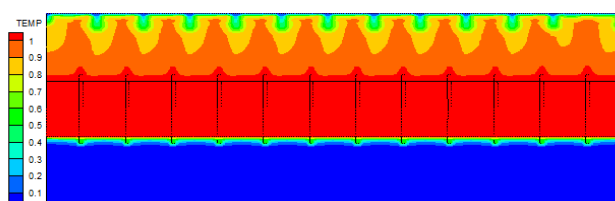


b. isotherms ( left), streamlines (right)

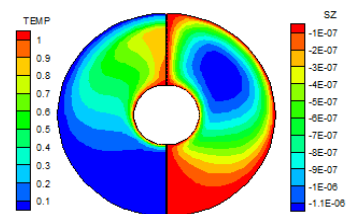


c. Axial velocity along annulus length

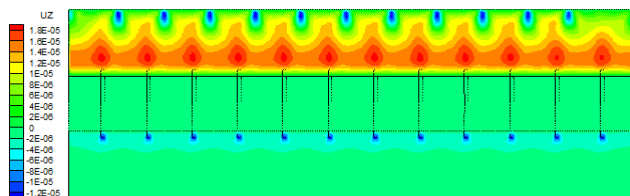
Figure. (3) Ra=500, a=0 and  $\phi=0$ .



a. Isotherms along annulus length

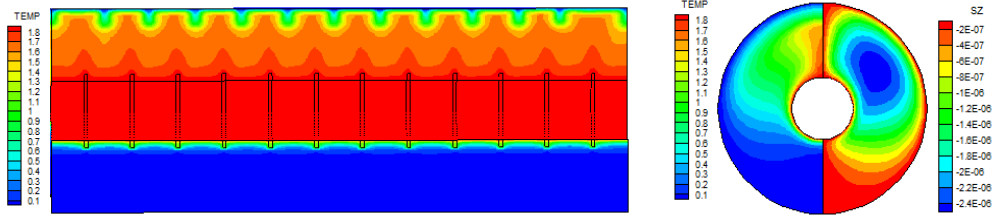


b. isotherms (left), streamlines (right)



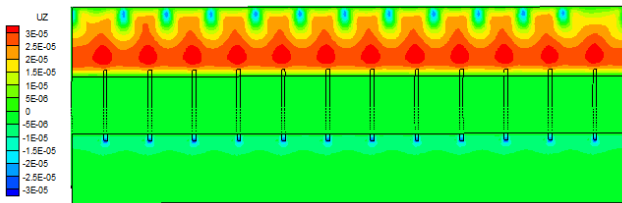
c. Axial velocity along annulus length

Figure. (4) Ra=500, a=0 and  $\phi=0.3$ .



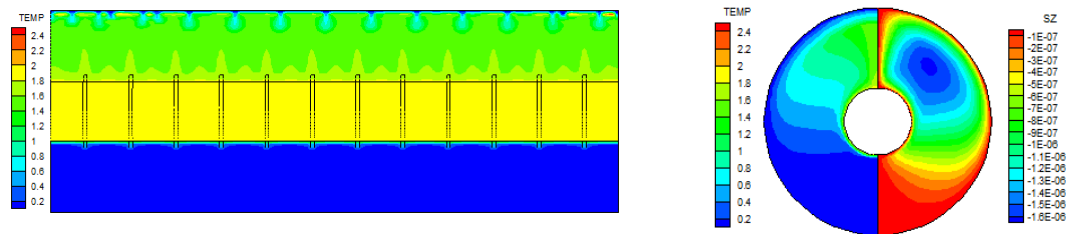
a. Isotherms along annulus length

b. isotherms (left), streamlines (right)



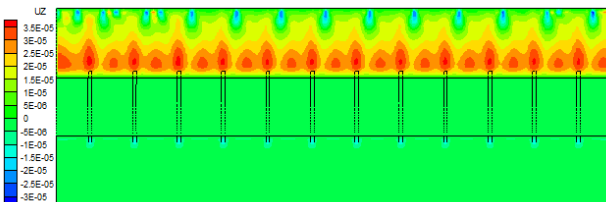
c. Axial velocity along annulus length

Figure. (5)  $Ra=500$ ,  $a=0.8$ ,  $\eta=0.01$  and  $\phi=0$



a. Isotherms along annulus length

b. isotherms (left), streamlines (right)



c. Axial velocity along annulus length

Figure. (6)  $Ra=500$ ,  $a=0.8$ ,  $\eta=0.01$  and  $\phi=0.3$

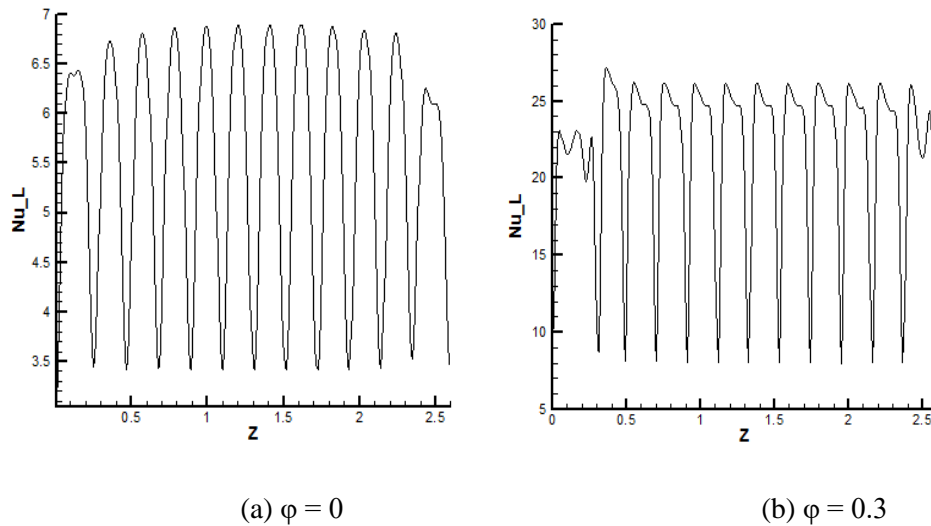


Figure (7) The variation of Local Nusselt number along the length of the inner cylinder for  $Ra^*=500$  and for constant wall temperature boundary condition ( $a=0$ ).

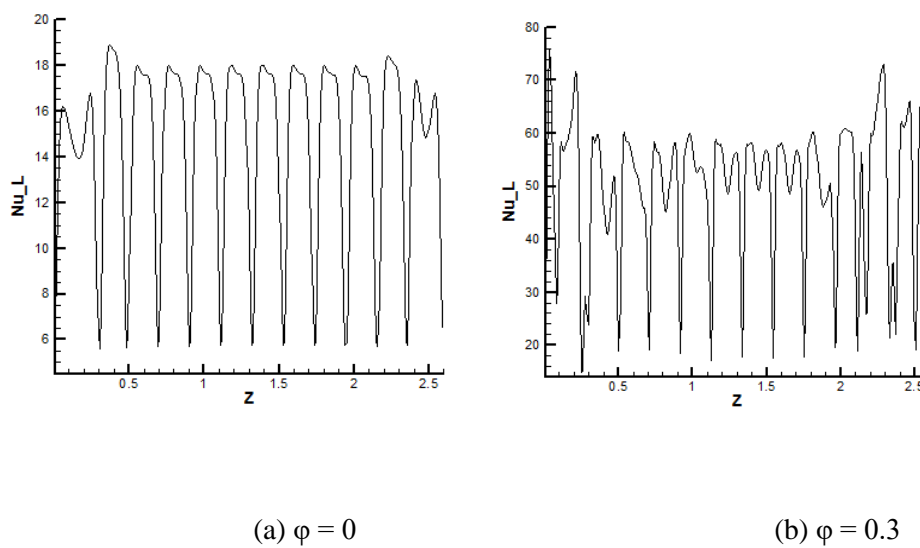
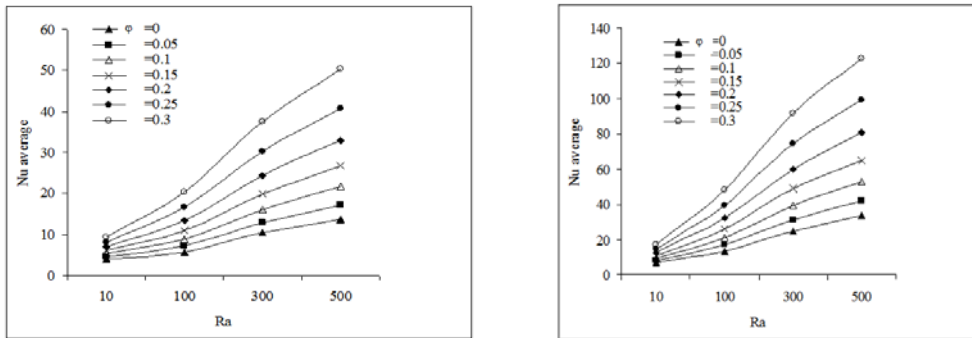
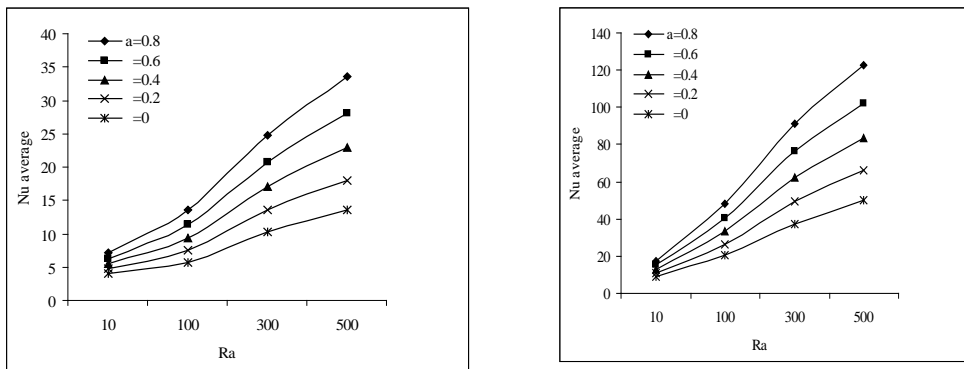


Figure. (8) The variation of Local Nusselt number along the length of the inner cylinder for  $Ra^*=500$  and sinusoidal oscillation temperature boundary condition ( $a=0.8$ ).



(a) Dimensionless amplitude (a) =0      (b) Dimensionless amplitude (a) =0.8

**Figure. (9) The variation of the average Nu with the modified Rayleigh number for various volume fractions ( $\phi$ )**



(a)  $\phi = 0$

(b)  $\phi = 0.3$

**Figure. (10) The variation of the average Nu with the modified Rayleigh number for various dimensionless amplitudes (a)**

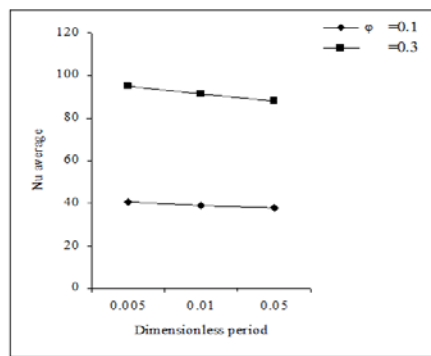


**Figure. (11) The variation of the average Nusselt number with the dimensionless period  $\hat{\eta}$  for dimensionless amplitude  $a=0.8$  and  $Ra^*=300$ .**

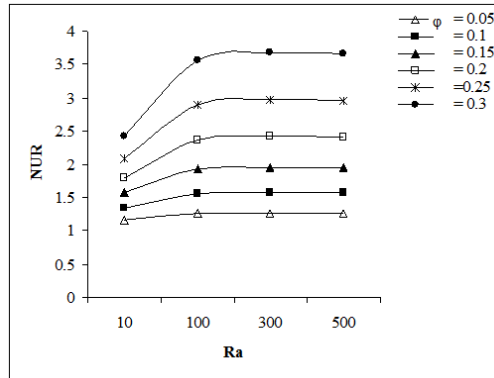


Figure. (12) The variation of the Nusselt number ratio with the modified Rayleigh number for various volume fractions ( $\phi$ ) and  $a=0.8$

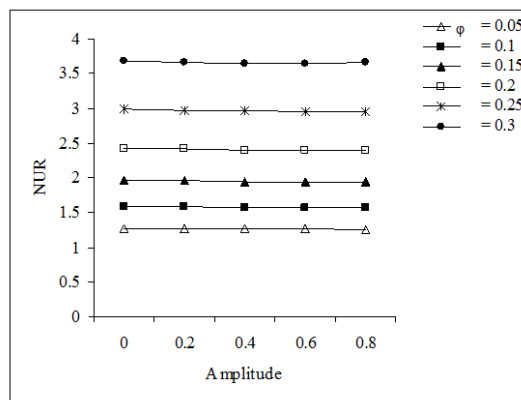


Figure. (13) The variation of the Nusselt number ratio with the dimensionless amplitude ( $a$ ) for various volume fractions ( $\phi$ ) and  $Ra^*=500$